American Mineralogist, Volume 92, pages 621–630, 2007

Transmission electron microscopy study of magnetites in a freshwater population of magnetotactic bacteria

A. ISAMBERT,[1] N. MENGUY,[2,*] E. LARQUET,[2] F. GUYOT,[2] AND J.-P. VALET[1]

[1]Laboratoire de Géomagnétisme et Paléomagnétisme, UMR 7577, Institut de Physique du Globe de Paris, Paris, France
[2]Département de Minéralogie, Institut de Minéralogie et Physique des Milieux Condensés, UMR CNRS 7590, Université Denis Diderot, Université Pierre et Marie Curie, et Institut de Physique du Globe, Paris, France

ABSTRACT

A freshwater population of magnetotactic bacteria has been extracted from the Seine River (France) and studied using transmission electron microscopy. Seventeen different morphotypes were recognized using morphological criteria, which rely on the number of magnetite crystals and their organization within cells, the size and shape of the cells and their statistical distribution. This study revealed new features in some magnetotactic bacteria that have not been described in the literature. In addition X-ray energy dispersive spectroscopy and electron diffraction analyses revealed cells containing Ba-rich and CaO inclusions. Two major modes of magnetite crystals growth were derived from the distributions of the crystal shapes in this population. Numerous cases of crystals elongations along axes different from the [111] axis are related to one singular process of crystal growth. Thus, this population of magnetites collected from cells extracted from the Seine River does not meet some of the criteria for biogenicity, which have been used so far for biomagnetites, particularly those concerning the [111] elongation axis.

Keywords: Magnetotactic bacteria, biogenic magnetite, crystal growth, transmission electron microscopy, biomineralization, crystal morphology, magnetosomes, morphotype census, morphology of biomagnetite, CSD

INTRODUCTION

Magnetotactic bacteria mineralize magnetosomes, which are nanometer-sized magnetite (Fe_3O_4) (Frankel et al. 1979) or greigite (Fe_3S_4) crystals (Heywood et al. 1990, 1991; Mann et al. 1990) in intracellular vesicles. The sizes, morphologies, crystallographic characteristics, and chemical compositions of the biogenic crystals of magnetite are controlled by the bacteria and are thus used as potential signatures of their biologic origin. Magnetosomes are generally arranged in chains with the easy magnetization axis of each crystal (corresponding to the [111] crystallographic axis of magnetite) aligned parallel to the chain. The chains, parallel to the motility axis of the cells, act as compass needles so that the bacteria tend to align passively along the Earth's magnetic field lines (Blakemore 1975). This phenomenon called magnetotaxis, coupled with flagellar motility and aerotaxis, allows the cells to locate and maintain an optimal position in vertical chemical gradients within aquatic environments.

These motile Gram-negative prokaryotes, ubiquitous in aquatic environments (Flies et al. 2005a), are cosmopolitan in distribution and are most frequently found in the oxic-anoxic transition zone (OATZ) (Flies et al. 2005b). They include coccoid, rod-shaped, vibrioid, and spirilloid (helical) forms. The habits of magnetite crystals appear to be consistent within a given strain (Meldrum et al. 1993a, 1993b), although some variations in shape and size can occur within single magnetosomes chains (Bazylinski et al. 1994). Bacterial magnetites display restricted width to length ratios (*w*/*l*) corresponding to the stable single-magnetic-domain (SD) size range (Moskowitz 1995). In addition to the cuboctahedral habits synthesized by spirilla, the most common morphologies are prismatic, tooth, and bullet-shaped (Bazylinski et al. 1993; Mann et al. 1987a, 1987b). Small and rounded crystals are common at the end of the chains and interpreted as immature crystals. They indicate that growth of the chain is produced by precipitation of new magnetosomes from the extremities.

In this paper, we studied magnetite crystals from a freshwater population of magnetotactic bacteria, extracted from a natural environment in the Seine River (France) using high-resolution transmission electron microscopy. Measurements of the width to length ratio of the magnetite crystals within individual cells led us to identify different growth processes. We observed also structural and morphological anomalies in some biomagnetite crystals that could question some of the biogenicity criteria used to determine the origin of nanometer-sized magnetite in sediments.

EXPERIMENTAL METHODS

The freshwater magnetotactic bacteria were collected from a calm and sandy riverside of the Seine River (Bray sur Seine, Seine et Marne, France), from November 2003 to June 2004 to cover a large range of temperatures. The pH was about 7.1 and water temperatures varied between 10 and 25 °C. Sampling was done at the water-sediment interface by filling 500 mL jars with approximately 40% sediment,

* E-mail: Nicolas.Menguy@impmc.jussieu.fr

TABLE 1. Magnetotactic morphotypes observed in the Seine River

	Size (µm)		Number of magnetite chains	*n* Number of crystals per cell	Crystals morphology	Crystals mean sizes (nm)		*N*	V_{mean} ($\cdot 10^{-22}$ m^3)	*M* ($\cdot 10^{-16}$ Am^2) magnetic moment	*n*·*M* ($\cdot 10^{-15}$ Am^2) magnetic moment per cell
	l	*w*				*l*(σ) length	*w*(σ) width				
RS A	~4	~2	1	~30 aligned irregularly	elongated prismatic	90(27)	56(18)	85	3.5(2.0)	1.8(1.0)	5.3(3.0)
RS B	~6.5	~2.5	2	~100	elongated prismatic	84(31)	59(21)	178	4.0(3.2)	2.0(1.6)	20.3(16.5)
RS C	–	~1.5	1	~30	elongated prismatic	75(32)	56(25)	67	3.7(4.0)	1.9(2.0)	5.6(6.0)
RS D	~4	-	1	~30	elongated prismatic	91(32)	58(22)	34	4.2(2.8)	2.1(1.4)	6.3(4.3)
RS E	~4	~1	1	~30	elongated prismatic	88(28)	64(23)	29	4.7(3.5)	2.4(1.7)	7.2(5.2)
RS F	~3	~1.5	1 multiple chain	~100	tooth-shaped	110(33)	41(4)	240	2.0(0.8)	1.0(0.4)	10.0(4.1)
RS G	~1.5	~0.5	1	~5 to 10	bullet-shaped	100(34)	43(4)	17	2.0(0.8)	1.0(0.4)	1.0(0.4)
RS H	–	–	1	17	tooth–shaped	93(28)	49(5)	14	2.4(1.0)	1.2(0.5)	2.0(0.9)
RS I	~12	~4	3 to 5 multiple chains	~1000	elongated prismatic	–	–	–	–	–	–
MC A	Ø ~2.5		4 (2 doubles chains)	~50	cubic	92(24)	87(23)	104	8.4(6.0)	4.2(3.0)	21.2(15.0)
MC B	Ø ~1 to 2		2	~10	prismatic	88(22)	75(20)	25	5.7(3.2)	2.9(1.6)	2.9(1.6)
MC C	Ø ~1.5		4 (2 doubles chains)	~35	elongated prismatic	68(21)	52(16)	35	2.3(1.4)	1.2(0.7)	4.1(2.6)
MC D	Ø ~1 to 4		clusters or irregular chains	~120	elongated prismatic	89(21)	57(14)	245	3.3(1.6)	1.7(0.8)	20.1(10.0)
MS A	~3	~0.5	1	17	cuboctahedral	58(14)	54(13)	16	1.0(0.5)	0.5(0.2)	0.9(0.4)
MS B	~3.5	~0.5	1	23	cuboctahedral	52 (7)	49(8)	23	0.7(0.2)	0.4(0.1)	0.8(0.3)
MS C	~3	~0.5	1	13	elongated prismatic	76(10)	50(7)	13	2.0(0.7)	1.0(0.3)	1.0(0.3)
MV A	~1.5	0.5	1	10	elongated prismatic	58(18)	43(19)	10	1.5(1.2)	0.7(0.6)	0.7(0.6)

Note: σ = standard deviation.

40% overlying water and 20% air. Bottles were taken back to the laboratory and shaken. The south pole of a cylindrical bar magnet, located next to the external side of the jars, allowed us to enrich magnetotactic bacteria. Magnetic cells were then removed with Pasteur pipettes and separated from remaining non-magnetic particles and cells using magnetic separation columns (MiniMACS OctoMACS, Miltenyi Biotec). Drops of purified magnetic samples were then deposited onto copper grids covered by a carbon thin film for the transmission electron microscope (TEM) observations.

Electron micrographs, used for statistical analysis of size and shape of magnetites, were obtained at low dose (~10 e$^-$Å^{-2}) on a Philips CM 120 transmission electron microscope (TEM) equipped with a LaB_6 gun. High-resolution electron microscopy (HREM) was performed on a JEOL 2100 F and a JEOL 2010 F equipped with a GATAN 794 digital camera. TEM photomicrographs stored onto a Kodak SO 163 film were digitized at high resolution (1000 to 4000 dpi) with a Nikon ED 8000 scanner for image analysis. The morphological studies of the crystals were carried out from the selected area electron diffraction (SAED) pattern analysis for isolated particles and from the Fast Fourier Transform (FFT) of HREM images for the smallest ones. As crystals are viewed in projection, the shape of nanocrystals of magnetite is not easy to determine (Buseck et al. 2001). Because the present study is focused on the elongation axis of crystals, we used stereographic projections to illustrate the crystallographic orientation deduced from the FFT of the HREM image. X-ray Energy Dispersive Spectroscopy (XEDS) analyses (probe diameter in the range 2–10 nm) were performed on the JEOL 2100 F TEM (counting time: ~300 s). The magnetite-bearing cells were studied by comparing the sizes and shapes of the magnetic cells and by characterizing the different types of intracellular reserve bodies. Subsequently, the size and shape of the intracellular magnetite particles were statistically analyzed to quantify their distributions. We measured the length (*l*) and half-length width (*w*) of a total of 1129 crystals from 32 magnetic cells. These dimensions correspond to the major and minor axes of the best-fitting ellipse, which has area and dimensions less than or equal to those of the crystal. The shape factors, describing the elongation of the crystals, were calculated from their width to length ratio, so that $w/l \leq 1$. The results are presented using histograms (Devouard et al. 1998) for each type of magnetic cell in Appendix 1.[1] As additional information, the magnetic dipole moment of the various cell types has been estimated. Calculations have been performed using the mean number and volume of crystals for each morphotype, and approximating the crystals shapes as rectangular prisms with square cross-sections for prisms and tooth and bullet-shaped crystals, and as spheres for cuboctahedral magnetite.

RESULTS

Seventeen morphotypes were defined principally on the basis of the morphology and size distribution of magnetite crystals, then combined with the disposition and arrangement of the crystals within cells, and finally with the size and shape of the magnetite-bearing cells. They are labeled and listed in Table 1. Each morphotype is designated by a code relative to the cell morphology and used in previous literature: RS for rod-shaped, MC for magnetococci, MS for magnetospirillum, and MV for magnetic vibrio.

Rod-shaped bacteria

Nine rod-shaped morphotypes were observed. These bacteria are by far the most abundant type present in our samples. They are also the largest magnetic cells with lengths ranging from 1.5 to 12 µm for the largest cells, and widths ranging from 1 to 4 µm. Among the collected rod-shaped bacteria, we detected the RS I type, which is very similar to the previous descriptions of *Magnetobacterium bavaricum* (Spring et al. 1993; Vali et al. 1987). This species is indeed easily recognizable by the fact that these large rod-shaped magnetic cells, up to 12 µm in length, may contain more than 600 magnetosomes in a unique cell, arranged in 3 up to 5 bundles of magnetosomes chains with various magnetite morphologies. Moreover, they contain many large reserve globules rich in sulfur, as previously described (Hanzlik et al. 2002).

Some singular characteristics were deduced from the compo-

[1] Deposit item AM-07-010, Appendix. The shape factors, describing the elongation of the crystals, were calculated from their width to length ratio, so that $w/l \leq 1$. The results are presented using histograms. Deposit items are available two ways: For a paper copy contact the Business Office of the Mineralogical Society of America (see inside front cover of recent issue) for price information. For an electronic copy visit the MSA web site at http://www.minsocam.org, go to the American Mineralogist Contents, find the table of contents for the specific volume/issue wanted, and then click on the deposit link there.

sitional analyses of intracellular inclusions of the RS-typed cells, which were not described so far in previous studies dealing with magnetotactic bacteria. RS F type measures about 3 µm in length and 1.5 µm in width. These cells contain 50 to 100 tooth-shaped magnetite crystals arranged in a multiple chain (Fig. 1a). The size of crystals ranges in length from 29 to 180 nm, and in width from 24 to 48 nm, with average length and width (standard deviation) of 109(33) and 41(5) nm respectively (N = 240). Their width to length ratio is 0.45(16). In addition, these cells harbor numerous small spherical inclusions of about 100 nm in diameter. From XEDS measurement, these electron dense bodies were shown to be rich in barium and calcium, with small amounts of phosphorus, sulfur, silicon and chlorine, commonly found in magnetic bacteria (Fig. 1b). Presence of Ba is normally not expected in classical intracellular inclusions of magnetotactic bacteria. Only occurrences of titanium, gold, and silver have been reported in literature (Keim and Farina 2005; Taylor et al. 2000). Barium was exclusively detected in the RS F-typed cells.

A second type of singular spherical bodies was observed in the RS H cells, which can be distinguished from RS F as they

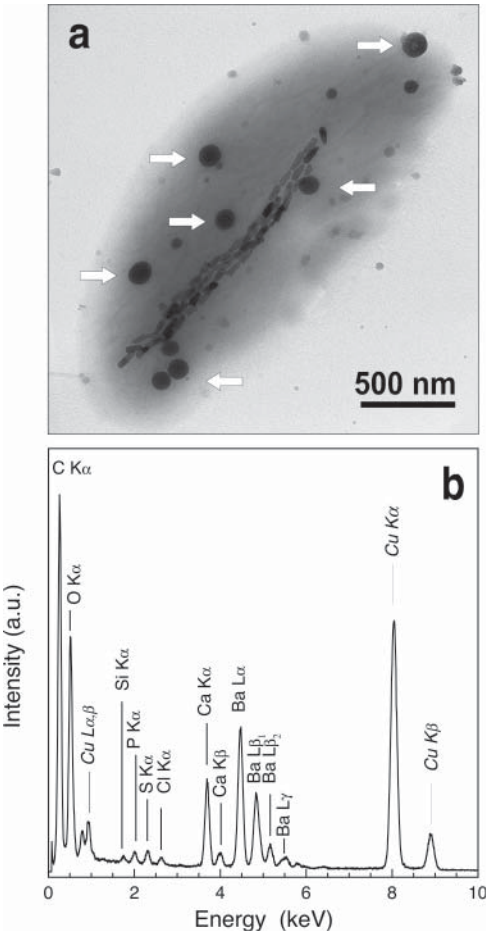

Figure 1. (**a**) TEM image of an RS F cell containing spherical electron dense intracellular inclusions. (**b**) XEDS analysis of one globule (white arrows) showing the important presence of calcium and barium.

contain only about 15 magnetites (Fig. 2a). The length of crystals ranges from 41 to 144 nm, while their width ranges from 40 to 56 nm, with average length and width (standard deviation) of 93(28) and 49(5) nm, respectively (N = 14). The width to length ratio is 0.57(17). Furthermore, these cells contain globules of about 200 nm in diameter (Fig. 2a). SAED analyses and XEDS measurements indicated that the spherical Ca-rich bodies consist of CaO nanocrystals with an average size of about 10 nm (Figs. 2b, 2c, and 2d). SAED patterns, taken before and after XEDS measurements to check for the absence of decarbonation of an amorphous carbonate under the electron beam, did not suggest any beam damage. We were not able to unambiguously determine from the TEM observations whether these spherical concretions were internal or external structures. However, XEDS analysis revealed that the surrounding environment in direct contact with these globules contains Na, Mg, Si, P, S, Cl, K, and Ca as for the RS F bacteria (Fig. 2e), suggesting a close relationship between these globules and the cell. Although it was previously observed in microbial fossil objects (Hladil and Gemperle 2004), presence of CaO in wet and cold conditions is very unusual. It normally results from high-temperature calcination of calcium carbonates ($CaCO_3$) and hydrates spontaneously upon contact with water to give the hydrated component $Ca(OH)_2$. Such unexpected CaO mineralizations were exclusively detected in the RS H cells.

The magnetite crystals mineralized by the RS cells exhibit various morphologies including classical elongated prismatic (Fig. 3a) and tooth and bullet-shaped crystals (Fig. 3d) with lower w/l ratios. Two major distributions of crystal morphologies are easily distinguishable (Figs. 3b and 3e). Most prisms show shape factors ranging from about 0.55 to 0.8. The smallest superparamagnetic magnetites found at the end of the chains and interpreted as immature, exhibit a prismatic morphology with mean w/l ratios of about 0.7, similar to larger crystals (Fig. 3c). Tooth or bullet-shaped magnetites show very different size and shape distributions. The smallest crystals are characterized by rounded shapes (Fig. 3d), with w/l ratio close to 1, very different from mature elongated magnetites with w/l around 0.25 (Figs. 3e and 3f). Figure 4 illustrates this phenomenon by showing the magnetite crystals of the RS H cells at different growth stages. Interestingly, a continuous change in shape is observable up to a critical size of about 45 nm. The smallest magnetites exhibit a near perfect sixfold symmetry along the <111> zone axis (Fig. 4b). This projected shape is compatible with a cuboctahedral morphology, i.e., with developed {111} and {110} faces. The larger crystals (Fig. 4c) are slightly elongated, but the existence of {110} faces can nevertheless be deduced from the projected shape. Only one developed {110} face is unambiguously visible in the magnetite shown in Figure 4d, while the conclusion is not straightforward regarding the other {hkl} faces. The crystal displayed in Figure 4e exhibits the same width as the mature ones but a significantly smaller length.

Magnetococci

Four morphotypes of magnetococci were observed in the samples (see Appendix 1). The sizes of these bacteria range between 1 and 4 µm, the majority of the observed cells measuring about 2 µm. Magnetites in these cells are all prismatic. Among the magnetococci population of this study, one type (MC D) is morphologically very close to the ARB-1 strain (Cox et al. 2002)

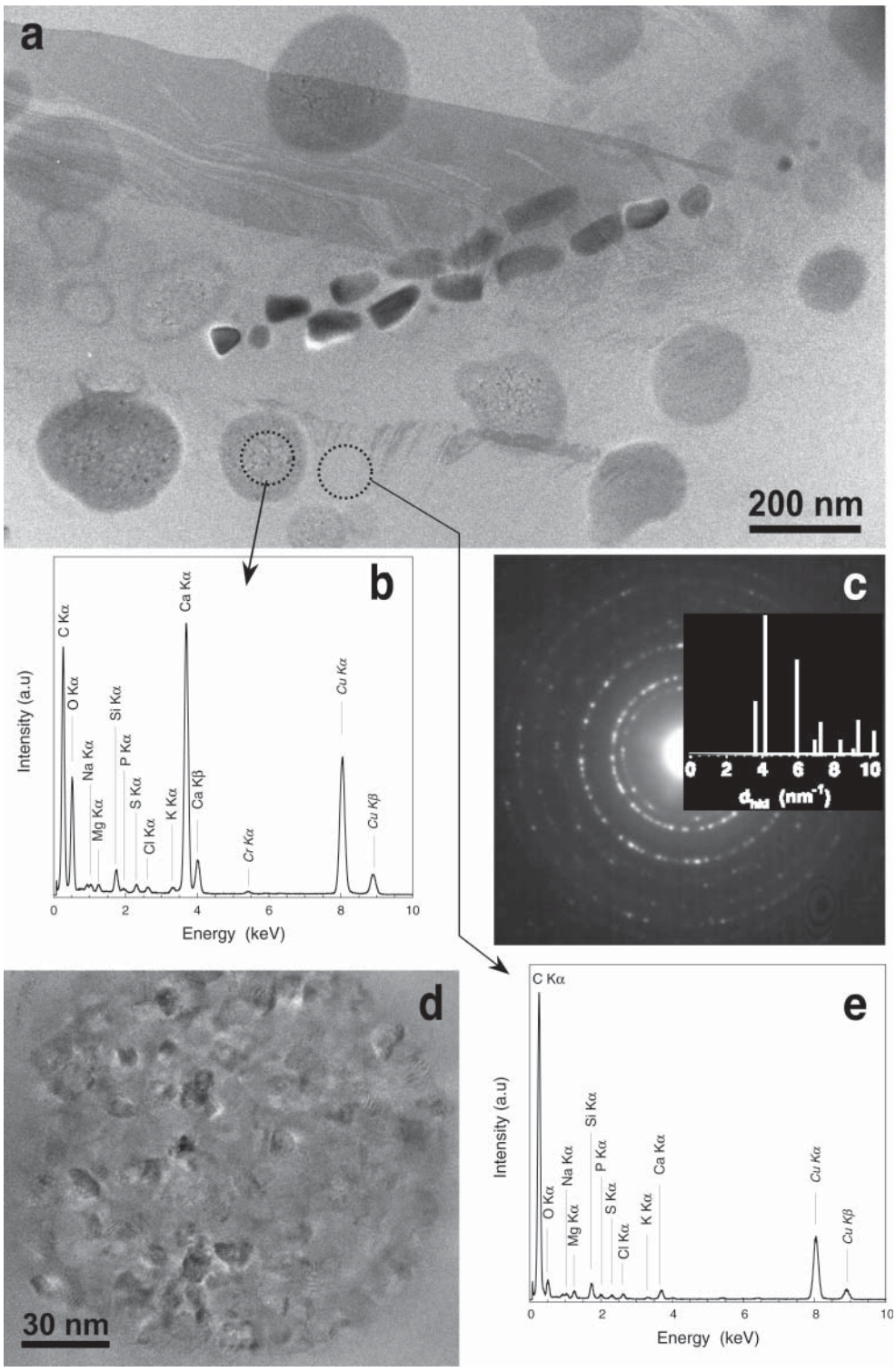

FIGURE 2. (**a**) TEM image of a double chain of magnetites and electron dense globules in an RS H cell. (**b** and **e**) XEDS analyses corresponding respectively to globule and surrounding environment revealing the presence of calcium in globules. (**d**) High-magnification image of one of the globules showing a nanocrystalline structure (diameter of the globule 250 nm) and corresponding SAED pattern with superimposed theoretical CaO electron powder diffraction diagram (**c**).

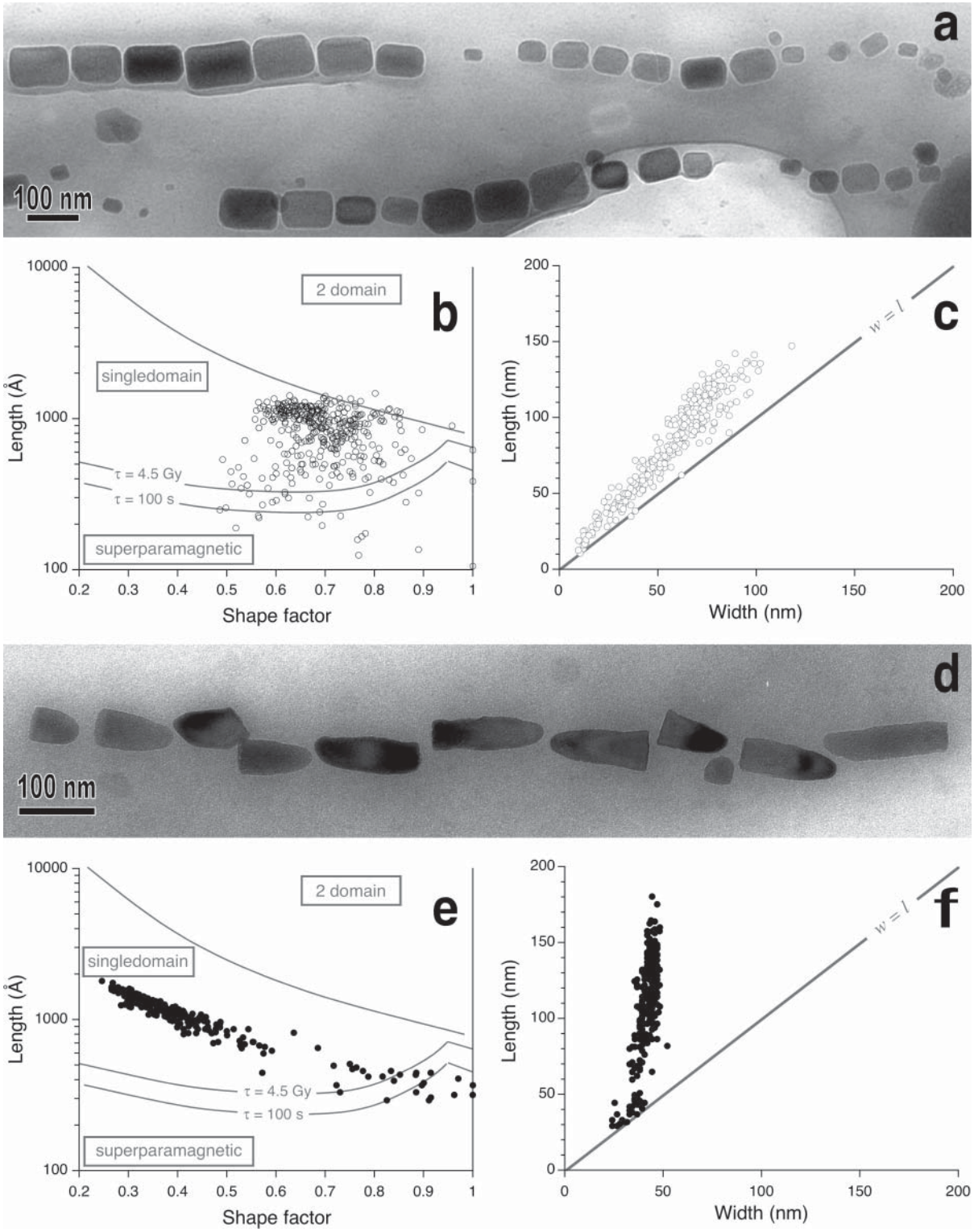

FIGURE 3. Size and shape distribution of magnetite crystals observed in the cumulated rod-shaped types. (**a**) TEM image of crystals mineralized by the RS B species. The smallest crystals show a constant shape factors <1. (**b**) Length as a function of shape factor for prismatic crystals. Boundaries between magnetic single-domain and superparamagnetic stability fields were drawn according to the calculations of Butler and Banerjee (1975). (**c**) Length vs. width of magnetite observed in the cumulated rod-shaped with prismatic crystals. (**d**) TEM image of bullet-shaped crystals mineralized by the RS G type. The smallest crystals at the end of the chain are rounded with shape factors *w*/*l* ~1. (**e**) Length as a function of shape factor and (**f**) length vs. width of magnetite observed in the cumulated rod-shaped with tooth and bullet-shaped magnetites.

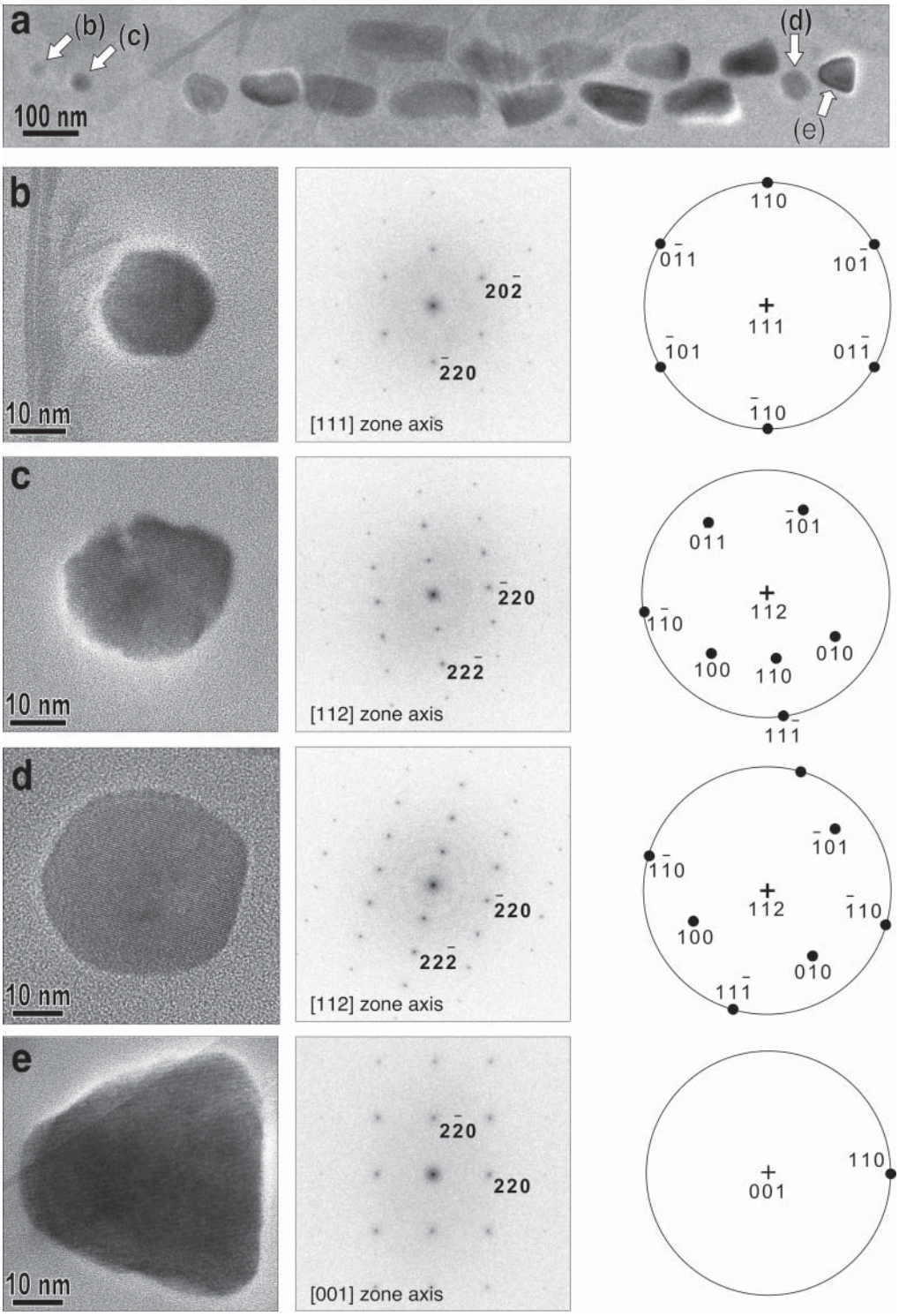

FIGURE 4. TEM observations of the magnetites of the RS H cells at different growth stages. (**a**) Overall view of the magnetite chain. The magnetites observed at higher magnification are labeled with respect to the following figures. (**b**–**e**) HREM observations of the magnetites labeled on **a**, their corresponding FFT and the stereographic projections oriented with respect to the FFT and HREM images. On each stereographic projection, the poles related to possible magnetite faces are plotted.

(Fig. 5). The cells are spherical with sizes from 1 to 4 µm (2.5 µm average). They contain two large phosphorus-rich symmetrical intracellular bodies and globules rich in sulfur. MC D contains about 120 prismatic magnetites occurring in irregular chains or clusters. The length of crystals varies between 22 and 120 nm while their width is between 13 to 81 nm, with average length and width of 89(21) and 57(14) nm, respectively (N = 245). The mean width to length ratio is 0.64(7).

Magnetospirillum

Three types of magnetospirillum were detected (see Appendix 1). The cell dimensions are ~3 µm in length, 0.5 µm in width. Magnetite crystals are relatively few (10 to 20 per cell) in comparison with most other magnetic cells. The magnetites that are mineralized by the MS bacteria show cuboctahedral and elongated prismatic morphologies (Fig. 6). Most cuboctahedral magnetites from the MS B bacteria are at the limit of the superparamagnetic state. This anomaly is balanced by the fact that crystals are arranged in chains, which stabilizes the cells magnetization. Such chains behave indeed approximately as stable single-domain bar magnets with very low shape factor values (<0.1) (Bazylinski et al. 1993; Carter-Stiglitz et al. 2003; Hanzlik et al. 1996, 2002).

Magnetic vibrio

Only one magnetic vibrio-typed cell was identified. MV A, with 1.5 µm in length and 0.5 µm in width, was the smallest cell observed in this study. Magnetite crystals are few (10 per cell). MV A crystals are prismatic with dimensions that are lower than most prismatic magnetites mineralized by other magnetic cells. The sizes of crystals range in length from 30 to 83 nm, and in width from 15 to 68 nm, with average length and width of 58(18) and 43(18) nm, respectively (N = 10). The mean width to length ratio is 0.7(1).

Discussion

A key issue for this study is the definition of the 17 morphotypes presented in Table 1 (a detailed description of each morphotype is given in Appendix 1). Some criteria for distinguishing between two different cell phenotypes are listed as entries of the table (length and width of cells, number of magnetite chains, number of magnetite crystals per cell, magnetite crystal morphologies and mean sizes, estimated magnetic moment per cell...). An additional and major criterion of distinction was obtained by comparing the plots of the crystals width distribution, the crystal length vs. width and finally the length vs. shape factor (Fig. 3) (Devouard et al. 1998; Mann et al. 1987b; Moench 1988). These additional graphical representations were very useful to distinguish between types of cells, which exhibit similar mean sizes and shapes of their crystals (for example the RS A and RS D, see Table 1). The plots obtained for each type and shown in Appendix 1 can thus be a powerful tool to characterize the diversity of magnetic morphotypes collected from natural environments.

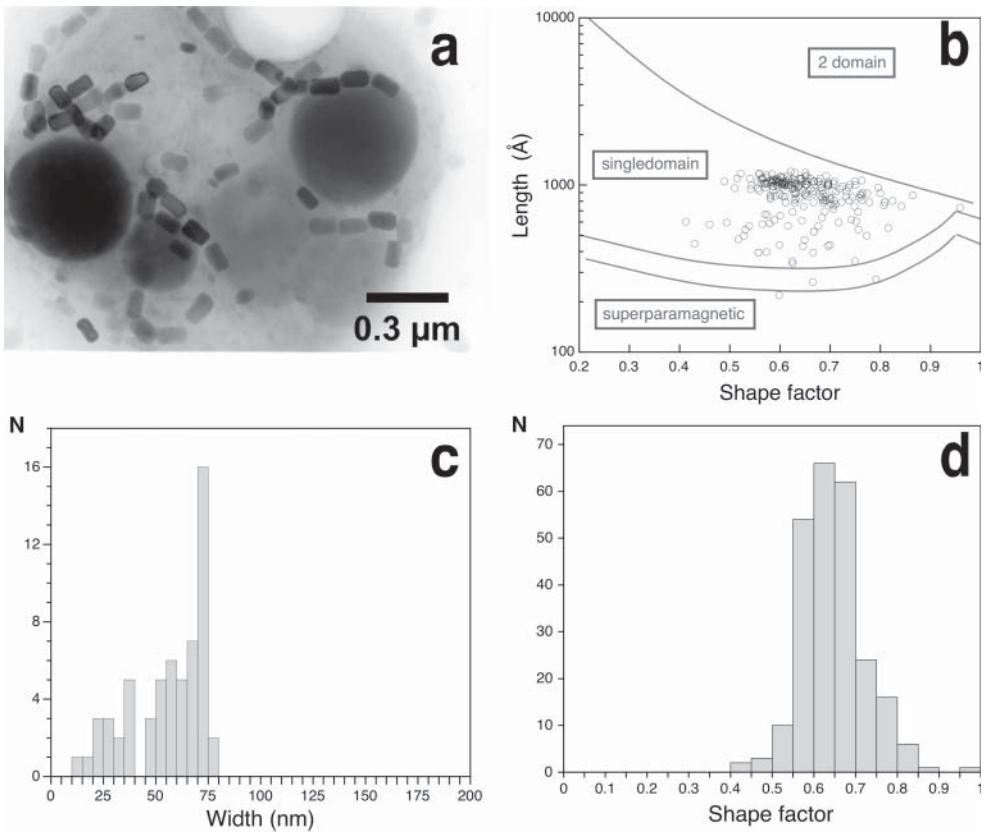

Figure 5. (**a**) TEM image of one cell of the MC D type resembling the ARB-1 bacteria. (**b**) Length vs. shape factor of 245 magnetite crystals observed in 5 cells. (**c** and **d**) Distributions of width and shape factors of the crystals from clusters and chains in this cell type.

Among the 17 phenotypes of cells, some were close to strains previously described (*Magnetobacterium bavaricum* and ARB-1), whereas most of them were observed at least once in the literature dedicated to magnetotactic bacteria (e.g., the MS and MC types). However, the present study allowed the detection of some phenotypes of magnetic cells showing new features. Indeed, RS F and RS H discovered in the Seine River contain singular reserve globules rich in barium and calcium oxide (CaO), respectively, which have not been reported previously in populations of magnetotactic bacteria.

Are the 17 cell types identified in this study 17 bacterial species? Could different species give similar phenotypes, which would not be considered as distinct types based on the criteria used in this work? On the contrary, could one given species correspond to several phenotypes? These important questions go beyond the scope of the present study. Further work should be done by combining the phenotypic criteria defined here with cultivation methods and cultivation-independent molecular techniques similar to the study conducted by Flies et al. (2005a). The present state of knowledge stipulates that the habits of magnetite crystals appear to be consistent within a given species (Meldrum et al. 1993a, 1993b), although some variations in shape and size can occur within single magnetosomes chains (Bazylinski et al. 1994). The simplest interpretation of our data would thus be that 17 distinct magnetotactic prokaryotic species were identified in the present sampling, but this remains to be studied further.

Magnetotactic bacteria are often associated with electron dense mineral globules. We observed several classical globules (e.g., the S-rich globules of *Magnetobacterium bavaricum* and the P-rich inclusions of the ARB-1 type cells) and other less standard globules—rich in Ba or composed of CaO. The interpretation of these globules, and even their exact localization (intracellular or at the vicinity of the cell surfaces) are far from being elucidated. However, if these peculiar globules (e.g., nanocrystallized CaO) are unique to the determined morphotypes, they could be used more systematically to distinguish between magnetic types of cells collected from natural environments. Moreover, they may open possibilities for using magnetotactic cells as environmental markers (e.g., accumulation of heavy metals such as Ba by magnetic cells).

The plots of magnetite crystals length vs. width or length vs. shape factor allowed us to refine the types of the magnetic cells. They also point to various crystal growth mechanisms in the different morphotypes. Two major trends of growth processes, closely linked to the crystals morphology, are easily distinguishable in RS-typed cells (Figs. 3c and 3f). Prisms show shape factors ranging between about 0.55 and 0.85 for the majority of the crystals. The smallest superparamagnetic magnetites also show a prismatic morphology , with w/l ratios similar to those of larger crystals (Figs. 3a and 3c). Thus, the distribution of length and width of prismatic magnetites from RS cells seems to follow the relation:

$$l = w/\alpha, \quad (1)$$

where α represents the mean shape factor (0.7). Regardless of crystal size, prisms exhibit a clear shape anisotropy, even for sizes as small as 10 nm. Homomorphic growth of the prismatic magnetite particles is likely in this case. Morphotypes showing tooth and bul-

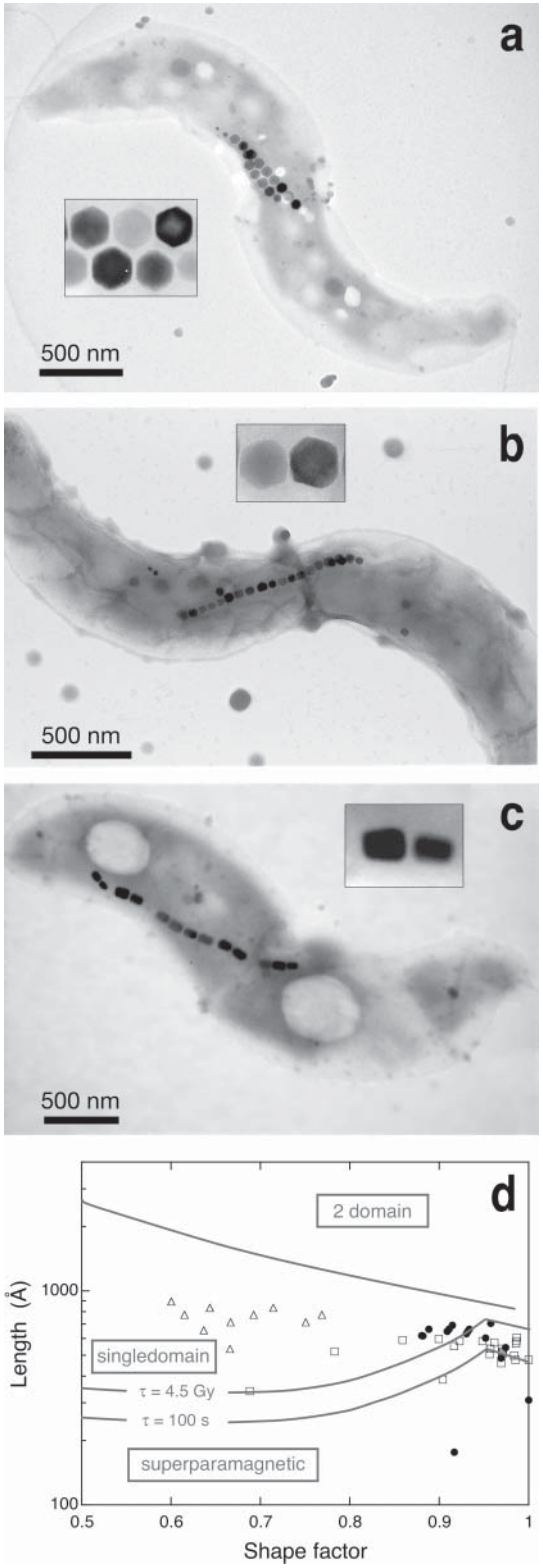

FIGURE 6. TEM images of the 3 magnetospirillum types observed in this study: (**a**) MS A, (**b**) MS B, (**c**) MS C. (**d**) Length vs. shape factor of the crystals. Triangles = prismatic crystals from MS C; dots = cuboctahedral crystals from MS A; and squares = cuboctahedral crystals from MS B.

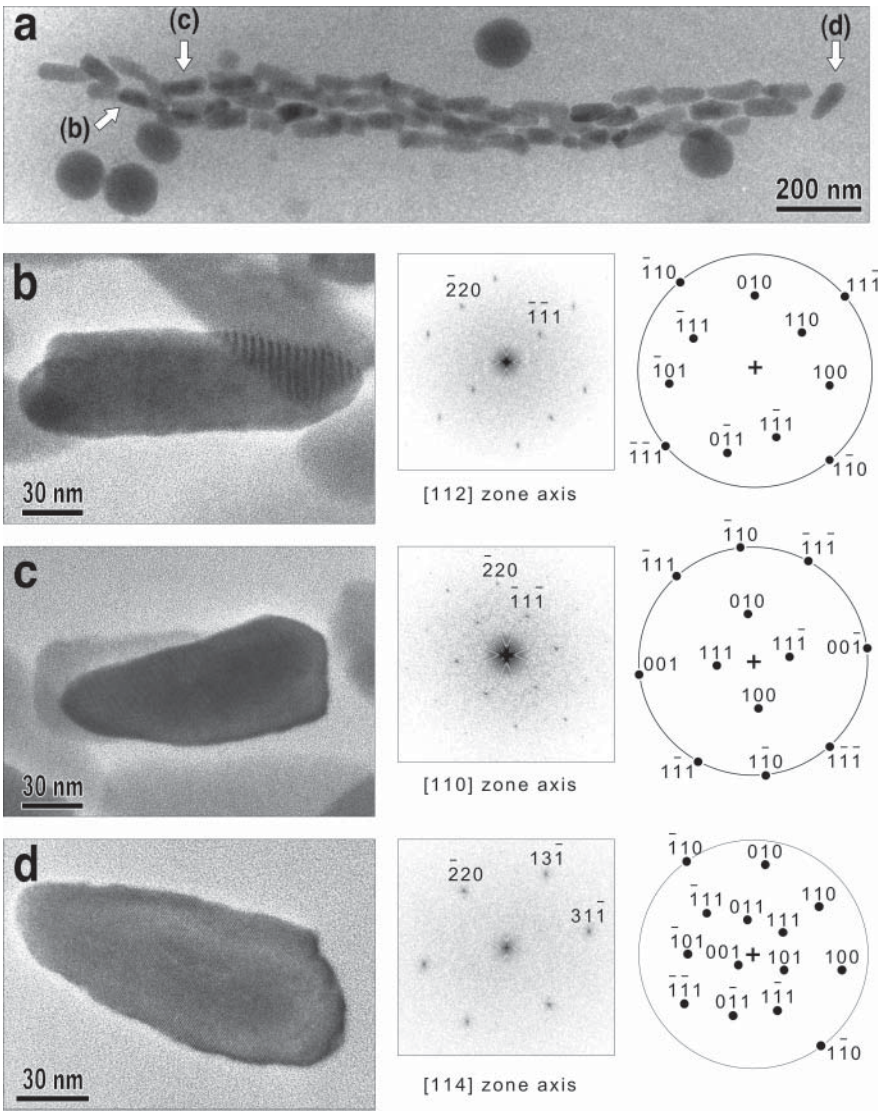

FIGURE 7. Morphology analysis of the RS F species magnetites. (**a**) Overall view of the magnetite chain. The magnetites observed at higher magnification are labeled with respect to the following figures. (**b**–**d**) HREM observations of the magnetites labeled on **a**, their corresponding FFT and the stereographic projections oriented with respect to the FFT and HREM images. On each stereographic projection, the poles related to main crystallographic directions are plotted. From these figures, it appears that the elongation directions of these magnetites is clearly not [111] but could be close to [100].

let-shaped crystals display a very different growth behavior (Figs. 3f and 4). Indeed, the smallest crystals are cuboctahedral with $\alpha = 1$. When crystals reach a width of about 45 nm, the growth mechanism changes abruptly. Crystals grow in length only , the width remaining constant (Figs. 3f and 4). A similar two-step growth for anisotropic magnetites has been suggested by Mann (1987b). This evolution could be considered as an adaptation to the magnetotaxis phenomenon, allowing the long needle-shaped particles to stay in the optimal magnetic single-domain size. The mechanism for this particular growth mode in tooth and bullet-shaped magnetites is still unknown but these observations suggest that it might be related to the contact between a growing magnetite crystal and a structure, involving probably a magnetosome membrane, which prevents magnetite growth in this direction.

Intracellular bacterial magnetites, resulting from highly controlled biomineralization processes, respond to specific morphological criteria. Among those, the crystallographic perfection and the elongation along the [111] easy magnetization axis of magnetite are usually used to distinguish between biogenic and inorganic crystals. In this study, we show that numerous biogenic magnetites are elongated along different axes than the [111] expected axis. Such exceptions have already been reported in literature for bullet-shaped crystals elongated in the [112] direction (Mann et al. 1987b; Meldrum et al. 1993b), arrowhead crystals, elongated in the [100] direction (Vali and Kirschvink 1989), magnetite whiskers (Taylor et al. 2000) and tooth-shaped magnetites, elongated in the [110] direction (Taylor and Barry 2004). Here we show that tooth-shaped magnetites can be elongated along a direction close to [100] axis (Fig. 7), which is close to the [114] axis proposed by (Hanzlik et al. 2002). Such anomalies can also be found, but more rarely, in prismatic magnetites, organized in chains of crystals mainly elongated along the [111] axis. Figure 8 shows such a chain with several [111] elongated prismatic magnetites including one not elongated along the [111] direction. The projected shape of this magnetite is compatible with an octahedron with poorly developed {100} and {110} faces (Figs. 8c and 8d). However, it can be seen that one [111] axis of this magnetite is almost aligned with the [111]

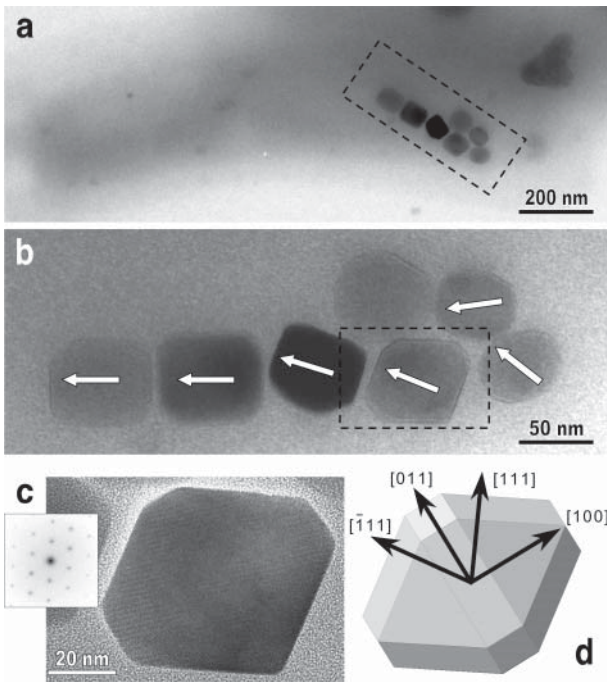

FIGURE 8. Observation of an anomalous morphology in a chain of elongated prismatic magnetites. (**a**) Overall view of the magnetite chain in the bacteria. (**b**) Close view of the magnetite chain. Arrows indicate the [111] crystallographic directions deduced from SAED patterns and FFT of HREM images and assumed to be the easy magnetization axis of each crystal. (**c**) HREM images of a magnetite belonging to the chain whose projected shape is compatible with an octahedron with poorly developed {100} and {110} faces labeled in (**d**).

axes of the surrounding magnetites. The elongation anomalies appear to be relatively frequent in tooth or bullet-shaped crystals populations synthesized by rod-shaped bacteria. These structural anomalies, which are not statistically negligible in a single population, would no longer have to be considered as exceptions to the usual biogenicity criteria. The [111] axis criterion would have to be used carefully. This phenomenon may be directly linked to the singular growth process of tooth-shaped magnetites. Additional observations are needed to investigate the way these irregular crystals are synthesized, which may be different from regular prismatic crystals, involving a classical magnetosome membrane (Hanzlik et al. 2002).

ACKNOWLEDGMENTS

We thank Damien Faivre for fruitful discussions. Part of this research was supported by the Bonus Qualité Recherche program of the Institut de Physique du Globe de Paris.

REFERENCES CITED

Bazylinski, D.A., Heywood, B.R., Mann, S., and Frankel, R.B. (1993) Fe_3O_4 and Fe_3S_4 in a bacterium. Nature, 366, 218.

Bazylinski, D.A., Garratt-Reed, A.J., and Frankel, R.B. (1994) Electron microscopic studies of magnetosomes in magnetotactic bacteria. Microscopy Research and Technique, 27, 389–401.

Blakemore, R.P. (1975) Magnetotactic Bacteria. Science, 190, 377–379.

Buseck, P.R., Dunin-Borkowski, R.E., Devouard, B., Frankel, R.B., McCartney, M.R., Midgley, P.A., Posfai, M., and Weyland, M. (2001) Magnetite morphology and life on Mars. Proceedings of the National Academy of Science, U.S.A., 98, 13490–13495.

Butler, R.F. and Banerjee, S.K. (1975) Theoretical single-domain grain size range in magnetite and titanomagnetite. Journal of Geophysical Research, 80(29), 4049–4058.

Carter-Stiglitz, B., Moskowitz, B., and Jackson, M. (2003) Correction to "Low-temperature remanence in stable single domain magnetite." Geophysical Research Letters, 30(21), 2113.

Cox, B.L., Popa, R., Bazylinski, D.A., Lanoil, B., Douglas, S., Belz, A., Engler, D., and Nealson, K.H. (2002) Organization and Elemental Analysis of P-, S-, and Fe-rich Inclusions in a Population of Freshwater Magnetococci. Geomicrobiology Journal, 19, 387–406.

Devouard, B., Posfai, M., Hua, X., Bazylinski, D.A., Frankel, R.B., and Buseck, P.R. (1998) Magnetite from magnetotactic bacteria: Size distribution and twinning. American Mineralogist, 83, 1387–1398.

Flies, C.B., Peplies, J., and Schüler, D. (2005a) Combined approach for characterization of unclultivated magnetotactic bacteria for various aquatic environments. Applied and Environmental Microbiology, 71, 2723–2731.

Flies, C.B., Jonkers, H.M., Beer, D.D., Bosselmann, K., Böttcher, M., and Schüler, D. (2005b) Diversity and vertical distribution of magnetotactic bacteria along chemical gradients in freshwater microcosms. FEMS Microbiology Ecology, 52, 185–195.

Frankel, R.B., Blakemore, R.P., and Wolfe, R.S. (1979) Magnetite in freshwater magnetotactic bacteria. Science, 203, 1355–1356.

Hanzlik, M., Winklhofer, M., and Petersen, N. (1996) Spatial Arrangement of Magnetosomes in Magnetotactic Bacteria. Earth and Planetary Science Letters, 145, 125–134.

——— (2002) Pulsed-field-remanence measurements on individual magnetotactic bacteria. Journal of Magnetism and Magnetic Materials, 248, 258–267.

Heywood, B.R., Bazylinski, D.A., Garratt-Reed, A.J., Mann, S., and Frankel, R.B. (1990) Controlled biosynthesis of greigite (Fe_3S_4) in magnetotactic bacteria. Naturwissenschaften, 77, 536–538.

Heywood, B.R., Mann, S., and Frankel, R.B. (1991) Structure, morphology and growth of biogenic greigite (Fe_3S_4), in Materials synthesis based on biological processes. In M. Alpert, P. Calvert, R.B. Frankel, P. Rieke, and D. Tirrell, Eds., p. 93–108. Materials Research Society, Pittsburgh, Pennsylvania.

Hladil, J. and Gemperle, A. (2004) CaO nucleation preceding carbonate growth in dying microbial particles (subsurface environment). Geochimica et Cosmochimica Acta, 68(11), Supplement (Goldschmidt 2004), A408 (abstract).

Keim, C.N. and Farina, M. (2005) Gold and Silver Trapping by uncultured Magnetotactic Cocci. Geomicrobiology Journal, 22, 55–63.

Mann, S., Sparks, N.H.C., and Blakemore, R.P. (1987a) Structure, morphology and crystal growth of anisotropic magnetite crystals in magnetic bacteria. Proceedings of the Royal Society of London B, 231, 477–487.

——— (1987b) Ultrastructure and characterization of anisotropic magnetic inclusions in magnetotactic bacteria. Proceedings of the Royal Society of London B, 231, 469–476.

Mann, S., Sparks, N.H.C., Frankel, R.B., Bazylinski, D.A., and Jannasch, H.W. (1990) Biomineralization of ferrimagnetic greigite (Fe_3S_4) and iron pyrite (FeS_2) in a magnetotactic bacterium. Nature, 343, 258–260.

Meldrum, F.C., Mann, S., Heywood, B.R., Frankel, R.B., and Bazylinski, D.A. (1993a) Electron microscopic study of magnetosomes in a cultured coccoid magnetotactic bacterium. Proceedings of the Royal Society of London B, 251, 231–236.

——— (1993b) Electron microscopic study of magnetosomes in two cultured vibriod magnetotactic bacteria. Proceedings of the Royal Society of London B, 251, 237–242.

Moench, T.T. (1988) *Bilophococcus magneticus* gen. nov. sp. nov., a motile, magnetic coccus. Anton Leeuw, 54, 483–396.

Moskowitz, B.M. (1995) Biomineralization of magnetic minerals. Reviews of Geophysics, 33, supplement (IUGG Report), 123–128.

Spring, S., Amann, R., Ludwig, W., Schleifer, K.H., Gemereden, H.V., and Petersen, N. (1993) Dominating role of an unusual magnetotactic bacterium in the microaerobic zone of a fresh-water sediment. Applied and Environmental Microbiology, 59, 2397–2403.

Taylor, A.P. and Barry, J.C. (2004) Magnetosomal matrix: ultrafine structure may template biomineralization of magnetosomes. Journal of Microscopy, 213(Pt 2), 180–197.

Taylor, A.P., Barry, J.C., and Webb, R.I. (2000) Structural and morphological anomalies in magnetosomes: possible biogenic origin for magnetite in ALH84001. Journal of Microscopy, 201, 84–106.

Vali, H. and Kirschvink, J.L. (1989) Magnetofossil dissolution in a paleomagnetically unstable deep-sea sediment. Nature, 339, 203–206.

Vali, H., Forster, O., Amarantidis, G., and Petersen, N. (1987) Magnetotactic bacteria and their magnetofossils in sediments. Earth and Planeteray Science Letters, 86, 389–400.

MANUSCRIPT RECEIVED APRIL 4, 2006
MANUSCRIPT ACCEPTED OCTOBER 30, 2006
MANUSCRIPT HANDLED BY KATRINA EDWARDS